Journal of Information Systems Engineering and Management
2025, 10(10s)
e-ISSN: 2468-4376
https://www.jisem-journal.com/

Research Article

A Novel Hybrid Optimization Tuned Deep-Long Short-Term Memory Model in COVID-19 Chest CT Image Segmentation

Dr. G. Jose Moses[1*], Dr. Kovvuri N Bhargavi[2], Tanaya Ganguly[3], Manoj kumar padhi[4], Ashwin.M[5], Dr. Velagapudi Sreenivas[6]

[1*]*Professor of CSE,School of Engineering,Malla Reddy University Hyderabad, Telangana, India*
josemoses@gmail.com

[2]*Associate Professor&HOD, Department of CSE-AIM, Aditya University,India*
kovvuri@acet.ac.in

[3]*Assistant Professor, Department of CSE*
Amity University, Ranchi, Jharkhand, INDIA
gangulytanaya11@gmail.com

[4]*Assistant professor,Department of Computer Science & Engineering,Centurion University Of Technology And Management,Paralakhemundi,Odisha, India*
manojpadhi1503@gmail.com

[5]*Professor,Department of Information Science and Engineering,AMC Engineering College, Bengaluru, Karnataka, India.*
mailmeashwin@gmail.com

[6]*Professor, Department of Computer Science and Engineering, SRK Institute of Technology Vijaywada-A.P, India*
velagapudisreenivas@gmail.com

ARTICLE INFO

Received: 18 Nov 2024

Revised: 24 Dec 2024

Accepted: 15 Jan 2025

ABSTRACT

Corona viral disease (COVID-19) has been declared a worldwide pandemic due to its fast spread. In order to prevent future infection and to protect lives, early detection of COVID-19 cases is crucial because failure to do so might result in death. The segmentation of patient COVID-19 chest computed tomography (CT) image data is proposed in this study using the tuned Deep Long Short-Term Memory (Deep-LSTM) classifier by Grey Wolf Grasshopper Optimisation (GWGHO). The proposed model segmentation accuracy is enhanced by applying the recommended approach to tune the Deep-LSTM weights optimally. The suggested method is created by combining the characteristics of grasshoppers and grey wolves in such a manner as to inherit both animals' benefits in solving optimisation challenges. By applying the GWGHO algorithm's tuning procedure, the convergence is also improved. The suggested GWGHO-Deep LSTM model's efficacy is confirmed by an investigation of the model's performance indices, including segmentation accuracy, recall, precision, and Area under curve (AUC). The suggested GWGHO-Deep LSTM model's segmentation accuracy was achieved at 97.5226%, demonstrating the effectiveness of the model in segmenting data.

Keywords: COVID-19, Chest CT image, Deep LSTM, Segmentation, and Optimization

1. Introduction

The most crucial components of the human respiratory system are the lungs. The total air circulation system is impacted by lung illness, which has the potential to cause mortality. Lung cancer, tuberculosis, and pneumonia are the other major lung diseases [12]. In addition, some microbes, such bacteria, viruses, and fungi, can cause illness that requires medical attention [1]. More than 200 nations have been affected by the extremely contagious and communicable illness COVID-19 during the past year. On the other hand, COVID-19 has expanded globally and is to blame for mortality, heart infections, and respiratory issues. The global economy has also suffered as a result of COVID-19. According to the study, the COVID-19 virus has a damaging effect on the lungs and swiftly mutates before the patient receives any diagnosis-based treatment [13][14][5]. More than 2 million confirmed cases, more than 150,000 fatalities, and other statistics have been reported as of April 2019. Early identification is essential since there

Copyright © 2024 by Author/s and Licensed by JISEM. This is an open access article distributed under the Creative Commons Attribution License which permitsunrestricted use, distribution, and reproduction in any medium, provided the original work is properly cited.

is no therapeutic cure or vaccination for the rare COVID-19 disease, making it necessary to immediately isolate the suspected patient and lower the risk of infection in the wider population [3].

A COVID-19 virus may be found in patients using a number of techniques, including the RTPCR test [15], X-ray imaging [16], CT scan [17], fast antigen [18], and serological test [19][5]. For respiratory or blood samples, RT-PCR or gene sequencing are the primary screening methods for COVID-19 [20]. According to reports, however, the overall positive rate of RT-PCR for samples taken from throat swabs ranges from 30 to 60%, leaving unidentified individuals who might infect a sizable population of apparently healthy people [21]. Chest radiography imaging utilising X-ray and computerised tomography (CT) is a commonly used method for diagnosing pneumonia and offers speedy findings. Chest CT has a high sensitivity for the diagnosis of COVID-19 [22], while X-ray pictures show visual indices related to COVID-19 [23] [3]. The COVID-19 chest imaging data, which was initially released in January 2020, showed that the majority of hospitalised individuals had bilateral pulmonary complications with ground-level opacities. Since then, several papers on the results of the COVID-19 chest CT have been published at a rapid rate.

Chest CT should be used properly in COVID-19 patients based on experience and, more importantly, scientific knowledge that has developed since the disease's emergence and is still growing [10]. Experts estimate that the COVID-19 virus has a one-week incubation period [24]. This is important because, during this period, the infected person acts as a viral carrier and unintentionally distributes the illness. Due to its very infectious nature, it spreads more quickly than it is discovered. Machine learning methods are particularly well-liked in healthcare applications [5]. In the present era, chest X-ray scans were utilised to predict COVID-19 using machine learning frameworks. The end-to-end deep learning structure is proposed, which forecasts COVID-19 disease using raw images without the need for feature extraction, in contrast to conventional techniques for medical image identification, which involve a two-step process, such as hand-crafted feature extraction and recognition [9]. It has been shown that deep learning-based models outperform traditional AI techniques in the majority of computer vision and medical image processing tasks [3]. They have been used to solve a variety of problems, from the recognition, segmentation, and recognition of faces to super-resolution and image enhancement.

Although various studies such as Deep Neural Network (DNN) [1], Deep transfer learning (DTL) [3], Residual Neural Network Version 50 (ResNet 50) [4], XCOVNet [5], Dilated Convolutional Neural Network (DiCNN) [6], Convolutional Support Vector Machine (CSVM) [7], Modified Convolutional Neural Network (MCNN) [8], Improved Deep Convolutional Neural Network (IDCNN) [37], and Automatic segmentation pipeline within 3-dimensional U-Net architecture (3D U-Net) [38] are conducted to classify the COVID-19 CT chest image, they face significant issues such as limited generalization, overfitting, computational complexity, lack of standardization, large false positive detection, etc. Therefore, to overcome the issues faced by these state-of-art techniques we proposed a novel hybrid optimization-based deep learning architecture for COVID-19 CT chest image classification.

This study presents a deep learning technique for segmenting the chest CT images of COVID-19 patients. The GWGHO technique is used to optimise the weights in the deep LSTM model, which effectively executes the segmentation process. The use of the GWGHO optimisation, which helps to increase the suggested segmentation model's effectiveness, is crucial to understanding the relevance of the presented model. The suggested segmentation model is well explained in this study, and the findings may be used to confirm the model's efficacy. Additionally, a thorough analysis of the effectiveness of the traditional segmentation procedures is provided to evaluate the superiority of the suggested method for segmenting chest CT images. The study's main contributions and subjects covered are,

- For the purpose of segmenting the COVID-19 CT images, the proposed algorithm creates an automated deep learning approach.
- The GWGHO method is used to optimise the Deep LSTM weights for better segmentation accuracy.
- The new model is compared to the existing methodologies in terms of efficiency measures like precision, accuracy, recall, and ROC curve to confirm the efficacy of the proposed strategy.

The paper is organised as follows: Section 1 provides a thorough introduction to the paper; Section 2 conveys a survey of current COVID-19 segmentation strategies and the difficulties they face; and Section 3 explains the proposed optimisation tuned deep learning framework for CT image segmentation. Section 4 discusses the outcomes of the suggested approach, and Section 5 concludes the article.

2. Literature survey

The usual techniques for COVID-19 CT image segmentation are discussed in this part, along with the problems with the current model that served as the impetus for the creation of the suggested model.

2.1 Related works

According to the literature evaluation of the available techniques, DeepikaSelvaraj *et al.*[1] suggested a deep neural network (DNN) model prepared on a small dataset, with features chosen using a region-specific technique based on the Zernike moment (ZM) and grey level co-occurrence matrix (GLCM). The difficulty in detecting the Ground-glass opacification/opacity (GGO) from low-contrast CT images is a shortcoming of this model, which necessitates the use of additional features and augmentation approaches to offer more precise information. For the goal of segmenting chest CT images with COVID-19 infections, Qingsen Yan et al. [37] created a special deep convolutional neural network (DCNN) model. A feature variation block is developed that adaptively modifies the global characteristics of the features for segmenting the COVID-19 infection. This is motivated by the finding that the border of the infected lung may be enhanced by modifying the global intensity. The FV block may efficiently and adaptably improve the capacity of feature representation for a variety of applications. However, the DCNN model requires large amount of data for better classification. For COVID-19-infected areas, Dominik Müller et al. [38] created an inventive automated segmentation workflow that can handle limited datasets by using variant databases. The technique was centred on the on-the-fly production of distinct and random picture patches for training using a variety of pre-processing techniques and considerable data augmentation. However, it is crucial to remember that the bulk of segmentation techniques used in research today are not appropriate for clinical use.

Deep learning methods were investigated by Shervin Minaeea et al. [3] in order to identify COVID-19 patients from CT scans. However, additional trials on the photographs are needed for a more consistent evaluation of these models' correctness because there are so few COVID-19 shots that have been made publicly available to far. Using a 1/7 Darwin COVID-19 Chest X-ray Dataset, Alan Zhang [4] trained a U-Net based network for lung-region segmentation as well as a convolutional neural network (CNN) for diagnosis on chest X-ray images. In order to identify COVID-19, VishuMadaan et al. [5] proposed a two-phase X-ray image classification model called XCOVNet using CNN. The front viewed fixed dimension X-ray pictures used to evaluate the XCOVNet model are used to produce filtered images, which may not be optimal and require more study and development. Using chest X-rays, Md Gulzar Hussain and Ye Shiren [8] evaluated CNNs for the classification of COVID-19. The method has limited sensitivity, latency, and accuracy [8]. Umut ozkaya1 *et al.* [7] suggested a Convolutional Support Vector Machine (CSVM) to classify CT images automatically. Shailender Kumar et al. [6] proposed a robust CNN framework for the identification of COVID-19 using Chest X-rays (CXR) as well as the images of Chest CT Scans with the goal to reduce the time it takes to identify infected persons. The dataset only contains a few COVID positive pictures, which hinders the effectiveness of the recommended CNN models [6].

2.2 Problem statement

The difficulties with the current COVID 19 CT image segmentation techniques are discussed as,

- Due to the reduced rate of publicly available COVID-19 images, more analysis are necessary on the larger set of clearly labeled COVID-19 images for the enhanced assessment of the accuracy of such models [2].
- An assessment method called sHapely Adaptive explanation (SHAP) does not offer causation. The strategy's behaviour and the information needed to construct the approach are the only details provided. Additionally, the technique may not accurately depict every COVID case, and a sizable number of false positives and negatives may be obtained [10].
- The presence of data anomalies, particularly in medical imaging operations, continues to be a bothersome problem that typically leads to misidentification among the different classes in the dataset [11].
- The decline in the size of input image due to the pooling layers of CNN can be handled with the addition of Transpose Convolutional layers, however adding such layers also raises the count of parameters, leading to the need for long training period [6].

3. Proposed model of COVID-19 chest segmentation

With the widespread spread of the corona virus, which causes an acute respiratory disease, the globe is currently plagued by a fatal sickness condition. Due to the high contagiousness of COVID, patients are advised to keep to themselves in order to stop the spread of the illness. To stop others from contracting COVID-19 and negatively impacting the nation's economy, quality of life, and way of life, the affected individuals must be located as quickly as feasible [1]. A novel hybrid optimization tuned deep LSTM model is projected in this article to part the chest CT pictures of the patient role affected through COVID-19 in such a way to direct early detection of COVID-19. The schematic depiction of proposed model is depicted in figure 1. In the initial step, the chest CT images are extracted from the dataset, and the extracted images are subjected to pre-processing for re-sizing and normalizing the input image. Then, the proposed hybrid optimization tuned Deep LSTM model involves in the segmentation of the pre-processed chest CT image. The Deep LSTM weights are optimised using the suggested GWGHO method, which contributes to improving the segmentation precision of the proposed model.

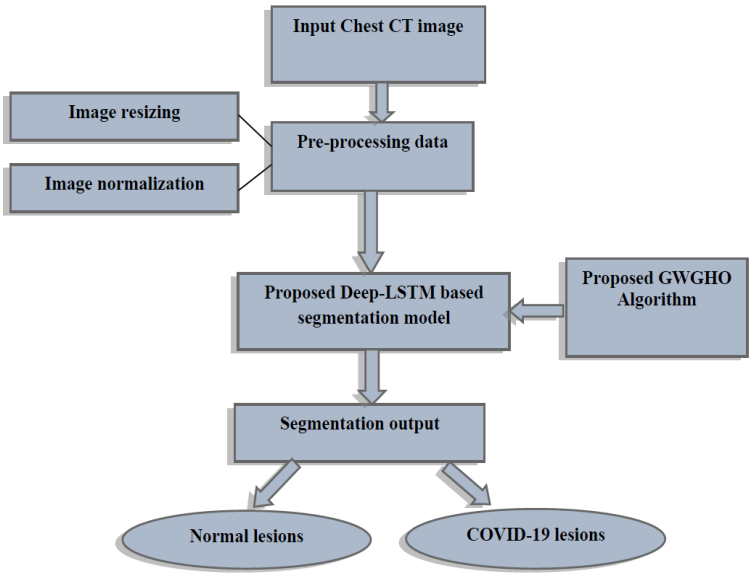

Figure 1. Block diagram of proposed Chest CT segmentation model

3.1 Input CT image

The segmentation of chest CT image is crucial in medical applications, due to the needs associated with it in enhancing the detection accuracy of the proposed segmentation module. Initially, the chest CT images are extracted from the input dataset, and is mathematically represented as,

$$E = \{CT_p\}; (1 \le p \le q) \tag{1}$$

Where, q refers to the total images of the input dataset and CT_p is the p^{th} image of the input dataset. The input images extracted from the dataset are processed in such a way to perform the segmentation process in the proposed research.

3.2 Pre-processing of image data

Pre-processing is one of the first phases in the planned COVID-19 chest CT image segmentation module's effort to remove artefacts from the CT images' nonlinear and non-stationary components [25]. The image obtained is considered to be pre-processed to improve the segmentation accuracy of proposed Deep LSTM model. To make the raw picture appropriate for subsequent processing, the pre-processing phase normalises it. All of the dataset's photos were downsized to 128 × 128 pixels as part of the pre-processing stage of the proposed model in order to speed up the training phase's processing time. To eliminate the abnormalities in the Chest CT pictures, all the images were also normalised.

3.3 Segmentation of chest CT image

The chest CT scan is routinely used to identify neurological diseases and check heart function. The CT is often acknowledged as a crucial step in evaluating clinical parameters, surgical planning, and particularly for the diagnosis of COVID-19 patients since it portrays critical components and structures from volumetric medical pictures. In a clinical environment, the doctor marks arcs around the structure of interest to define the area through the encircling tissues or organs. But because it takes longer and includes intra- and inter-rater variability, this method is inapplicable at a bigger footprint. As a result, it's critical to create a fully automated technique for segmenting and diagnosing medical images. Patches are employed as inputs instead of sending the entire image to the proposed setup because of the complexity inherent in chest CT imaging. The objective is the centre pixel/voxel, which the segmentation model segment using patches. Due to its capacity for identifying the position of the central pixel, the bigger patch provides spatial data. The smaller patch has a wealth of information about the region surrounding the core pixel. The proposed GWGHO optimisation tuned Deep LSTM model proposes segmenting the ideal segment of the chest CT image in order to simplify and improve the success of the subsequent classification procedure [26].

3.3.1 Proposed Brain CT image segmentation model based on optimized Deep Long Short-Term Memory network

The working principle of Hybrid optimization tuned Deep-LSTM model is explained in detail in this section. The proposed hybrid inspect optimization tuned Deep-LSTM model make in use of the pre-processed CT image in such a way to perform the segmentation process. The GWGHO method, which is proposed, and which incorporates the features of the grey wolf search agents and the grasshopper search agents, must be tuned optimally to get the best segmentation results. The Deep LSTM model has been demonstrated to be effective in processing non-linear higher order CT images, and the majority of segmentation models in the literature are based on deep learning. The Deep-LSTM is a collection of LSTM units that collect non-linear feature representations of various orders at varying depths in order to increase prediction performance [27]. However, the accuracy of segmentation is highly dependent on the weights of deep LSTM model being properly trained, leading to the invention of the GWGHO method, which combines the intrinsic qualities of grey wolf and grasshopper search agents.

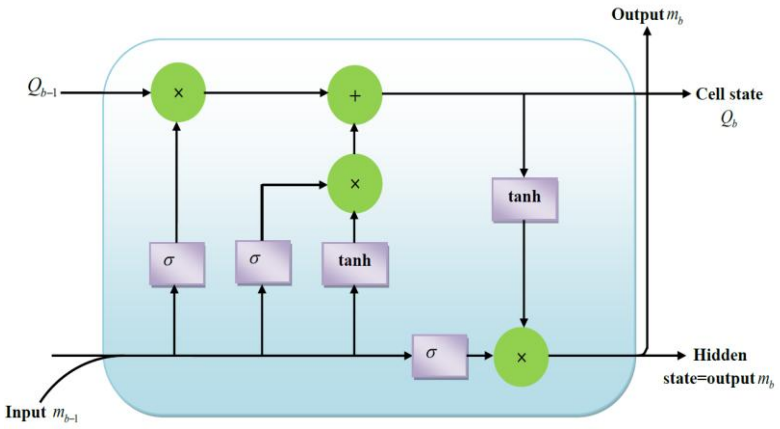

Figure 2. Architecture of LSTM model

a) Architecture of Deep LSTM: Recurrent networks of the LSTM type can successfully address the issue of vanishing gradient. The suggested brain CT image segmentation uses a deep recurrent network, also known as the Deep-LSTM network, which is made up of a number of LSTM network layers. The synthesized network takes full advantage of the major benefits of LSTM recurrent networks and deep networks. The state of the cells determines the Deep-LSTM neural network's output, which supports the proposed model in segmentation. In addition to recent data, the Deep-LSTM model takes into account substantial past inputs. As shown in figure 2, the memory cell, which is made up of many subunits with different goals, lies at the memory cell of the Deep-LSTM network's operation.

The input node m_b accepts data r_b from the deep network's input layer and the node's previous hidden states m_{b-1} in time instances. In order to increase prediction accuracy, the non-linear information used for prediction aids

the use of a deep LSTM model for the prediction of non-linear output in the presence of a non-linear element achieved by a sigmoid function.

As a result, the weighted summation of r_b and m_{b-1} is send with a $\tanh$ function, as follows:

$$N_b = \tanh\left(r_b \cdot M_{Nr} + m_{b-1} M_{Nm} + n_{inputnode}\right) \tag{2}$$

The input gate L_b is a unit sigmoid activation function that receives similar inputs, same as the input node. It's called that input gate as it obstructs inputs from new nodes from flowing to current node, resulting in a zero net value. It permits the values to flow only when the net measure is one [28]. The mathematical indication of the function is formulated as,

$$L_b = B\left(r_b \cdot M_{Nr} + m_{b-1} M_{Nm} + n_{inputgate}\right) \tag{3}$$

The internal state, denoted by Q_b is a node in the presence of a self-loop recurrent edge possessing unit weight and a linear activation function, denoted by

$$Q_b = L_r \cdot N_b + Q_{b-1} \tag{4}$$

The forget state, denoted as y_b, is a subunit for re-starting the memory cell's internal state and is expressed as,

$$y_b = B\left(r_b \cdot M_{mr} + m_{b-1} M_{ym} + n_{forget}\right) \tag{5}$$

The output gates R_b complete the task as follows in the end state:

$$R_b = B\left(r_b \cdot M_{Sr} + m_{b-1} M_{Sm} + n_{outputgate}\right) \tag{6}$$

The memory cell's final output is evaluated using the expression defined as,

$$m_b = \tanh\left(Q_b\right) \cdot R_b \tag{7}$$

Where, $Q_b = N_b \cdot L_b + Q_{b-1} \cdot y_b$.The construction of Deep LSTM is shown in Figure 3.

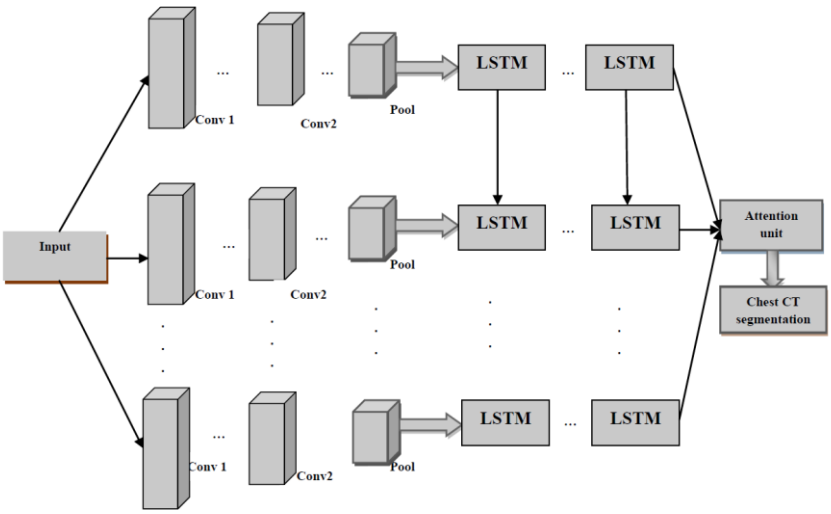

Figure 3. Construction of deep LSTM model

In the Deep LSTM based segmentation model's output, there is only one output layer. For the calculation of the weights, the suggested GWGHO technique is employed to train the Deep LSTM based segmentation model.

3.3.2 Proposed Grey wolf-Grasshopper optimization algorithm

The GWGHO optimization strategy is a hybrid form of meta-heuristic that blends grey wolf search agents' leadership and hunting hierarchy attributes [29] with grasshopper search agents' social qualities [30]. Standard optimizations are built around dynamic properties, meaning a proactive approach to dealing with convergence issues. The proposed GWGHO algorithm addresses this problem by leveraging the population's self-motivated characteristics in grey wolf search agents, which improves the proposed algorithm's ability to achieve a better global optimal solution than general optimization techniques, which are more likely to produce local optimal solutions.

a) Inspiration of proposed optimization algorithm:

The leadership and hunting grading traits of grey wolf search agents are coupled with the social traits of grasshopper search agents to create the cross meta-heuristics, which is a population-incorporated optimisation. The wolf inhabitants in this optimization lives in groups and is a member of the wolf family. The presence of grey wolf search agents in the ranking-based hunting characteristics, such as Leader grey wolf search agents, representative grey wolf search agents, obeyer grey wolf search agents, and scapegoat grey wolf search agents, ensures effective convergence. As previously stated, hierarchical levels enhance the grey wolf search agents' ranking-based hunting practice, with the Leader grey wolf search agent at the top of the hierarchy and in charge of developing solutions for resting and hunting states. The Leader grey wolf search agents leads the other grey wolf search agents when they are foraging, despite not being the strongest of the group and never mating within the pack. The second level of the rank, the representative grey wolf search agents, direct the Leader search agent by communicating the choice to the obeyer and scapegoat search agents. The scapegoat grey wolf search agents are still guarding the entire force at the lowest level. The obeyer grey wolf search agents are slightly higher than the scapegoat grey wolf search agents and are largely responsible for carrying out the directives of the Leader grey wolf search agents [29]. The main steps of the suggested GWGHO algorithm are as follows:

1) Social searching order
2) Adjoining operation
3) Grey wolf foraging hunting
4) Social authority operation
5) Phase of exploration

The following is a mathematical model of the GWGHO algorithm on the basis of the social dominance nature of grey wolf search agents and the social features of grasshopper search agents:

Mathematical design of proposed GWGHO optimization

The proposed GWGHO was utilized to optimally tune the Deep-LSTM parameters to improve the segmentation efficiency of the Deep-LSTM for COVID-19 lesion classification. The optimization process commence with the initialization of grey wolves and grasshoppers population, which potentially defines the hyperparameters such as weights, learning rate, batch size, etc., of Deep-LSTM. This method integrates the exploration capability of grey wolves with the exploitation capacity of grasshoppers to obtain effective and balanced search process. In the optimization process, the GWGHO approach explores the solution space to estimate the optimal hyperparameters for the Deep-LSTM model. It adjusts the hyperparameter sequence iteratively based on the model performance on the validation set. The aim of this fine-tuning process is to maximize the accuracy lesion segmentation and to reduce the false-positives and false-negatives. This algorithm dynamically adjusts its search parameters like convergence rate, population size, and exploration-exploitation trade-off to confirm maximum convergence to an optimal solution. This adaptively of the proposed technique helps to find the optimal hyperparameter sequence for the Deep-LSTM, reduces the issues like overfitting, and improves the generalization capacity of the proposed framework. The following is a summary of the mathematical model of grey wolf search agents at various stages:

a) Social searching order: The hierarchy of grey wolf search agents is made up of the Leader, representative, obeyer, and scapegoat agents, with the Leader agent being the most physically fit. The representative and obeyer grey wolf search agents, respectively, are the second and third best grey wolf search agents and are recognised as such, while the rest are viewed as the scapegoat grey wolf search agents.

b) Adjoining operation: The grey wolf search agents surround the prey in this phase based on its needs and convenience. The surrounding operation's grey wolf search agents are portrayed as,

$$G_{gd}^{s+1} = G_u^s - H.\psi \tag{8}$$

Where G_{gd}^{s+1} indicates the new location of g^{th} search agent on the d^{th} coordinate axis. Let $s+1$ denotes the prey's location, and ψ indicates the separation between the grey wolf search agents and the potential prey. The vector of distance is written as,

$$\psi = \left| P_1.G_u^s - G^s \right| \tag{9}$$

Where G^s denotes the grey wolf search agent's position in time s and P_1 represents the coefficient trajectory. Moreover, the coefficient trajectories, such as H and P_1 is systematically represented as.

$$H = 2i\ .j_1 - i \tag{10}$$

$$P_1 = 2\,j_2 \tag{11}$$

Where i gradually falls from 2 to 0 with the increase in iterations, j_1 and j_2 represents a random vector with a range of 0 to 1.

c) Grey wolf foraging phase: The grey wolf search agents have the ability to recognize prey, with the Leader search agent leading the foraging process, with the representative search agent and the obeyer grey wolf search agent joining in. The essential foraging behaviors of grey wolves are stated mathematically as,

$$\psi_\alpha = \left| P_1 G_\alpha - G \right| \tag{12}$$

$$\psi_\beta = \left| P_2 G_\beta - G \right| \tag{13}$$

$$\psi_\delta = \left| P_3 G_\delta - G \right| \tag{14}$$

During the foraging phase, $\psi_\alpha, \psi_\beta, \psi_\delta$ shows the current course of the most effective search agent for grey wolves. $P_1, P_2,$ and P_3 denotes the grey wolf search agents' random parameters that balance the periods of exploration and exploitation. When the location of the prey is closer to that of the grey wolf search agent, the prey is surrounded by the grey wolf search agents. During this procedure, the Leader grey wolf search agent formulates a command, based on which the representative grey wolf search agent instructs the other grey wolf search agents to forage the prey. The distance vectors are written as follows:

$$G_1 = G_\alpha - H_1 \psi_\alpha \tag{15}$$

$$G_2 = G_\beta - H_2 \psi_\beta \tag{16}$$

$$G_3 = G_\delta - H_3 \psi_\delta \tag{17}$$

Where $H_1, H_2,$ and H_3 are the coefficient vectors, and G_α represents the most excellent solution at the given time s. $H_1, H_2,$ and H_3 denotes the parameters that are tunable in the optimization procedure in responsibility of

achieving finest conjunction. In general, the first three best solutions based on Leader grey wolf search agents, representative grey wolf search agents, and obeyer grey wolf search agents [26] with respect to their positions as,

$$G_{gd}^{s+1} = \frac{G_1 + G_2 + G_3}{3} \tag{18}$$

Where, in the optimization process, G_1 is the location of the Leader grey wolf search agent, G_2 is the location of the representative grey wolfs, and G_3 is the position of obeyer grey, which refers to the first three best foraging places.

The Grasshopper search agents look for traits like hopping and rolling in a cylinder-like motion. The foraging features of the Grasshopper search agent may be found in both the nymph and developed states of the agent, which is a unique feature. In comparison to the mobility in the mature stage, the Grasshopper search agent moves slowly. The Grasshopper search agent's food searching function is divided into two sections to carry out the exploitation and exploration phases of operations. During exploration, the Grasshopper search agent searches globally, while during exploitation, the Grasshopper search agents searches inside the space for search locally. The leadership and hunting hierarchy traits of the grey wolf search agents are combined with the social traits of the grasshopper search agents to advance the convergence features of the grey wolf search agents [30]. The Grasshoppers search agents' position update equation is as follows:

$$G_{GHO}^{s+1} = G_4 = J\sum_{\substack{k=1 \\ j\neq l}}^{I} J\,\frac{U_t - V_t}{2}\, x\left|w_k^t - w_l^t\right|\left(\frac{w_k - w_l}{t_{lk}}\right) + \hat{K}_t \tag{19}$$

w_k is the k^{th} grasshopper search agent, and w_l is the l^{th} grasshopper search agent. U_t is the upper bound dimension, and V_t is the lower bound dimension, and $\hat{K}_t$ represents the t^{th} dimension value in the target. The distance among l^{th} as well as k^{th} grasshopper search an agent is a x function. The repulsion zone, attraction zone, and comfort zone all diminish as the coefficient J decreases. The typical equation for describing the position of the Grasshopper search agent is (20). Therefore, the position of the proposed GWGHO optimisation method is represented as, by combining the qualities of Grasshopper search devices and Grey Wolf search individuals.

$$G_{GWGHO}^{s+1} = \frac{G_1 + G_2 + G_3 + G_4}{4} \tag{20}$$

$$G_{GWGHO}^{s+1} = \frac{G_\alpha - H_1\psi_\alpha + G_\beta - H_2\psi_\beta + G_\delta - H_3\psi_\delta + J\sum_{\substack{k=1 \\ j\neq l}}^{I} J\,\frac{U_t - V_t}{2}\, x\left|w_k^t - w_l^t\right|\left(\frac{w_k - w_l}{t_{lk}}\right) + \hat{K}_t}{4} \tag{21}$$

As a result, the above equation closely resembles the position of the suggested GWGHO optimization technique, which aids in the optimal tuning of Deep LSTM parameters to improve segmentation accuracy.

d) Social authority operation: The grey wolf search agents are only seeking for prey in the hunt interplanetary in this phase, and they select the local ideal locations to assail the prey and finish the foraging procedure that is precisely described in terms of H changing between the intervals $-2j_1$ to $2j_1$ .The value of j_1 decreases from 2 to 0 with the increase in iterations. The position is updated based on the grey wolf search agents' social foraging rating and the satisfaction of the requirement $H < 1$.

e) Phase of Exploration: The grey wolf search agents, such as the Leader grey wolf search agent, representative grey wolf search agent, obeyer grey wolf search agent, and scapegoat grey wolf search agent, explore the solution outside of the space of solution and converge at the global optimal measure in this phase. The exploration phase fulfils the requirement $|H > 1|$ .The term P is in charge of ensuring that foraging abilities are improved. By rejecting

local optimal solutions and providing a global optimum solution, the proposed GWGHO optimization approach achieves a improved equilibrium among exploration and exploitation segments.

Algorithmic procedure of GWGHO algorithm: The step-wise clarification of proposed GWGHO procedure is as tracks:

i) Initialization: In the first stage, the population of the grey wolf search agent is initialised as the initial set of answers, which is provided by,

$$G_{gd};(1 \le g \le \eta);(1 \le d \le \gamma) \tag{22}$$

Where, η represents the number of grey wolf search agents in use, and is where they are located on the organize axis.

ii) Assessment of fitness performance: The highest possible value of accuracy obtained using the GWGHO algorithm is the fitness function of the proposed segmentation model. For the solution to be ideal and increase the efficacy of the suggested segmentation model, the value of fitness is anticipated to be maximum.

iii) Realization of best solution: Depending on the fitness measure, which is maximal over all iterations, the optimal solution is regarded as α, β and δ grey wolf search agents. The other grey wolf search agents become involved in the process of updating the position of the Leader grey wolf after the best options have been identified. Equation (21) is the updated equation for the suggested GWGHO optimisation strategies. It combines the traits of the search agents for grey wolf and the Grasshoppers.

iv) Coefficients updating: To maintain the proper stability between the exploration and exploitation steps, the coefficients of the optimisation process, including constants, parameters, and random metrics for optimisation, are adjusted.

Table 1. GWGHO algorithm pseudocode

Sl. No	GWGHO algorithm pseudocode
1	**Input:** $G_{gd};(1 \le g \le \eta);(1 \le d \le \gamma)$
2	**Output:** G_{GWGHO}^{s+1}
3	Create the population of the grey wolf search agents G_{gd}
4	Initialize the coefficients, ψ, j
5	Evaluate the fitness measure for all grey wolf search agents
6	For all ψ
7	{
8	G_{α} as best grey wolf solution
9	G_{β} as best grey wolf solution
10	G_{δ} as best grey wolf solution
11	}
12	While $s < s_{\max}$
13	{
14	Update the position as per equation (21)

15	}
16	End For
17	Update the coefficients, ψ, j
18	Evaluate fitness for all grey wolf search agents
19	Update the solutions $G_\alpha, G_\beta, G_\delta$
20	$s = s + 1$
21	}
22	EndWhile
23	EndFor
24	Return G_{GWGHO}^{s+1}

v) Termination: The process is carried out up until the worldwide best solution is identified. Table 1 displays the GWGHO optimisation algorithm's pseudocode. The utilization of exploration and exploitation benefits of GWGHO fine-tunes and improves the performance of the deep LSTM. In addition to this, several changes in the deep LSTM, architecture improves its performance in COVID-19 lesion segmentation. The changes includes integrating skip connection, attention mechanism's, multi-scale features, and dilated convolutions in deep LSTM architecture provides robust segmentation results. The integration of skip connections between the LSTM layers enables short route for data flow; this enables the model to learn about image features effectively by preserving and propagating gradients throughout the network. The incorporation of attention function allows the system to focus on extracting the spatial information from the image. This enables the deep LSTM model to dynamically weigh the various important image features correlative to COVID-19 lesion segmentation. Further, the introduction of multi-scale features makes the system to capture data at different levels, improving the segmentation performance. In addition, incorporating dilated convolutions in the deep LSTM increases the receptive field without increasing the parameter count. This allows to capture more contextual data from a larger region, leading to increased understanding of lesion structure by the model

4. Results and discussions

This section discusses the COVID-19 chest CT segmentation findings utilising the GWGHO-Deep LSTM approach..

4.1 Experimental arrangement

The suggested GWGHO-Deep LSTM model is tested using the MATLAB tool, which is fixed in Windows 10 and a 64-bit of operating system with 16GB of RAM.

4.2 Dataset description

The COVID segmentation Database [31] is utilised in the segmentation model that is suggested, which consists of 100 axial CT scans of individuals who are over 40 years old. The training pictures are 512x512 in size, as are the test images.

4.3 Evaluation indices:

The measures referred to as below metrics are used to gauge the performance of the GWGHO-based Deep LSTM model,

a) Accuracy: Training accuracy is the percentage of successfully segmented data out of the complete quantity of data processed for segmentation, as opposed to testing accuracy, which is the percentage of properly segmented data out of the total number of cases utilised for testing.

b) Precision: The term precision refers to the measure of quality, and system of higher precision provides more relevant outcomes as compared to irrelevant ones.

c) Recall: The term recall is a measure of quantity, and a higher recall measure represents that the system provides most of the relevant outcomes.

d) Area under curve: The area under ROC cure, abbreviated as AUC is a singular scale measure that evaluates the overall performance of the Deep LSTM model in segmentation process.

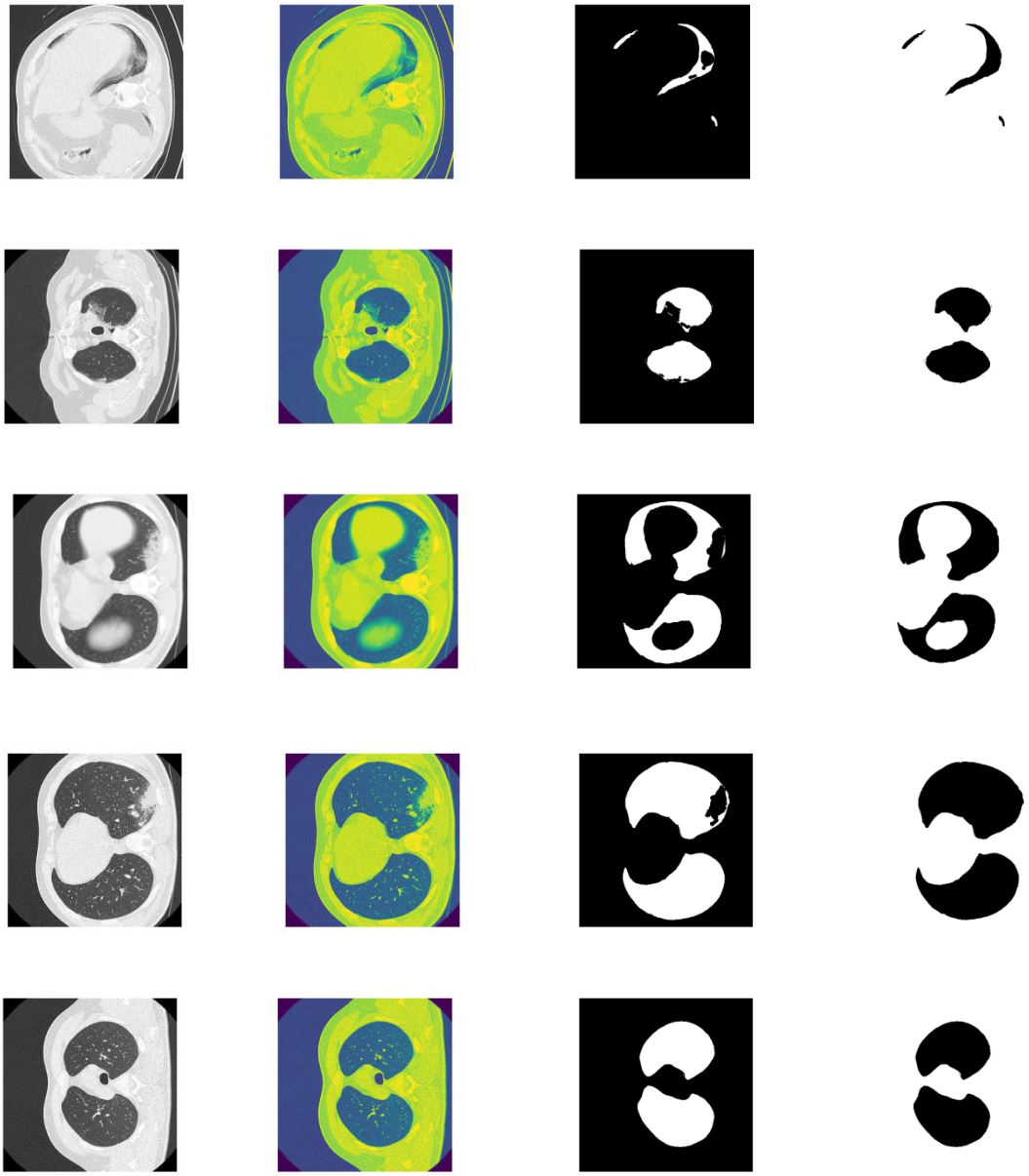

(a) **(b)** **(c)** **(d)**

Figure 4. Experimental results of the proposed segmentation model, (a) Original CT image, (b) Pre-processed image, (c) Ground truth image, and (d) Segmented image

4.4 Experimental results

The experimental outcomes of the proposed GWGHO-Deep LSTM segmentation model are portrayed in this section. The visual identification of the segmented image is depicted in figure 4. The original chest CT image, pre-processed image, ground truth image and the final segmented image are shown in figure 4. The segmented images are nearly equal to the ground truth image, which indicates the effectiveness of GWGHO-Deep LSTM in segmentation process.

4.5 Performance evaluation

The performance assessment of the GWGHO-Deep LSTM segmentation model is discussed in this part based on the performance indices of precision, accuracy, recall, and AUC. Utilising the training percent and k-fold value, analysis is performed.

4.5.1 Performance evaluation in terms of loss and accuracy

In this module, the convergence and robustness of the developed framework were examined by analyzing the accuracy and loss on training and validation dataset. The accuracy and loss are determined by increasing the number of iterations from 0 to 100. Figure presents the accuracy of the designed model on training and testing dataset. The training accuracy represents how well the proposed model functions on the training data sequence and it demonstrates how well it fits to the train set. Over the increasing number of iterations, the designed model achieved approximately 0.99 accuracy for the training dataset. This manifests that the developed model quickly captures the relationship between the data and correctly classifies the samples on the training set. The testing accuracy provides model performance on the test data sequence. It denotes how well the developed model can predict the COVID-19 lesions in chest CT images. It also defines the models generalization capacity to the unseen chest CT images. The designed approach attained an average testing accuracy of 0.97, which illustrates that this model can perform well on unseen dataset.

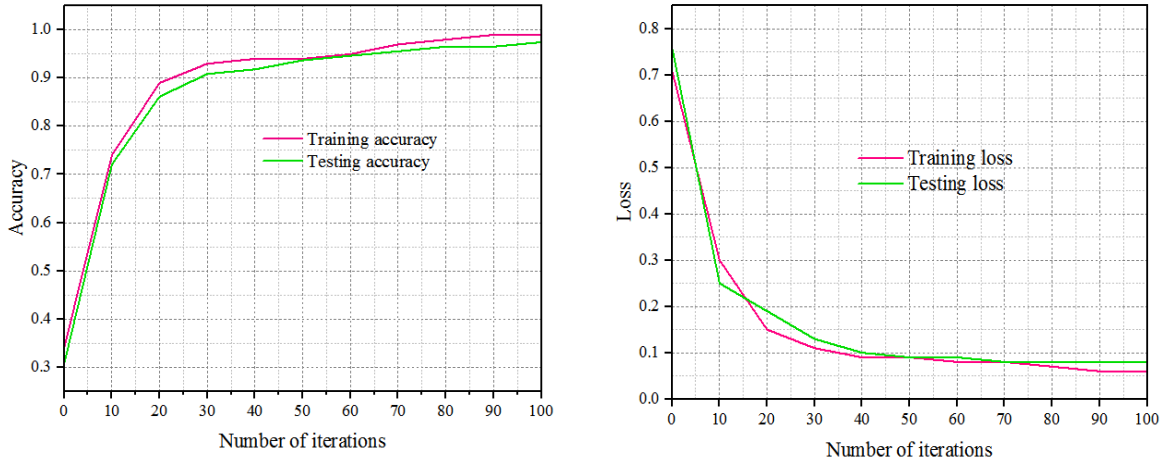

(a) (b)

Figure Performance evaluation: (a) accuracy, (b) loss

In addition, the training and validation loss were analyzed to evaluate the possibility of classification error in the proposed model. The training loss defines the error between the actual target labels and the detected output in training process. Figure presents the losses incurred by the proposed model. The presented model attained a lower training loss of 0.06, which defines that this framework efficiently adjusts its weights and other parameters to better approximate the ground truth labels. The testing loss measures the models generalization capacity and determines the variation between the actual and detected labels on unseen data samples. The proposed method earned less testing loss of 0.08, which describes that this approach performs well on unseen chest CT images and eliminates overfitting issue. The small deviation between the testing and training accuracy demonstrates good generalization and robustness of the developed model. Moreover, the designed model reaches stable and optimal performance during training quickly; this illustrates that the convergence speed of the model is fast and it quickly learns and adapt the patterns and interconnections between the data. This is achieved by integrating the hybrid optimization mechanism GWGHO for fine-tuning the Deep-LSTM approach. This fine-tuning enables the proposed model to reach its optimal segmentation accuracy quickly compared to the existing models. Furthermore, the computational requirements, resource utilization, training time, etc., of the developed model were examined. The computational time includes the time taken by the developed model for performing the computational tasks such as image pre-processing, optimization, fine-tuning, lesion segmentation, model training, and others. The computational complexity of the proposed work is tabulated in Table 2.

Table 2 Computational complexity

Tasks	Time (ms)
Image pre-processing	2.0
Optimization and fine-tuning	4.5
Deep LSTM training	4.0
Lesion segmentation	3.2
Other computational tasks (example: data loading)	1.1
Total computational time	14.8

To provide COVID-19 lesion segmentation, the developed model consumed total time of approximately 14.8ms, out of which the system consumes 2.0ms for image pre-processing, 4.5ms for optimization and fine-tuning of hyperparameters, 4.0ms for deep LSTM training, 3.2ms for lesion segmentation, and 1.1ms for performing other computational tasks. The minimum computational time illustrates that the designed model can process large volume of data precisely with less time consumption. However, the time consumption of the system increases over increase in dataset size. In addition, the computational requirements such as hardware resources includes accelerator's, GPUs, etc., increases over increase in dataset size. However, the hybrid optimization integrated in the developed continuously updates the hyperparameters of the training model, and reduces the computational requirements like memory, batch size, number of parameters, etc. Moreover, this integrated framework effectively optimizes the architecture, weights, and other parameters of deep LSTM, leading to improved resource allocation and utilization during both training and inference stages. Thus, with improved resource utilization, the model can effectively handle the computational demands associated with deep learning and LSTM architectures, even when dealing with large volumes of medical imaging data.

4.5.2 Performance evaluation in terms of training percentage

Figure 5 shows the GWGHO-Deep LSTM's performance in terms of precision, accuracy, recall, and AUC in terms of training%. In Figure 5(a), the accuracy analysis is presented. The accuracy of the GWGHO-Deep LSTM model is 92.4799, 93.3621, 93.8173, 94.9646, and 95.3256, respectively, with a training percentage of 60% and an epoch of 20, 40, 60, 80, and 100. The accuracy of GWGHO-Deep LSTM model for the training percentage of 70%, with the epoch of 20, 40, 60, 80 and 100 are 92.9549, 93.8385, 94.336, 95.4733, and 95.7251, respectively. The accuracy of GWGHO-Deep LSTM model for the training percentage of 80%, with the epoch of 20, 40, 60, 80 and 100 are 92.9791, 93.9554, 94.3486, 95.4954, and 96.1077, respectively. The accuracy of GWGHO-Deep LSTM model for the training percentage of 90%, with the epoch of 20, 40, 60, 80 and 100 are 93.0272, 94.2211, 94.3861, 95.5438, and 96.295, correspondingly.

The evaluation in terms of accuracy is shown in Figure 5(b). The precision of GWGHO-Deep LSTM model for the training percentage of 60%, with the epoch of 20, 40, 60, 80 and 100 are 78.1803, 79.5944, 80.8487, 88.2016, and 95.4263, respectively. The precision of GWGHO-Deep LSTM model for the training percentage of 70%, with the epoch of 20, 40, 60, 80 and 100 are 78.2647, 80.3482, 81.4227, 93.4477, and 96.0744, respectively. The precision of GWGHO-Deep LSTM model for the training percentage of 80%, with the epoch of 20, 40, 60, 80 and 100 are 80.2299, 80.7611, 82.5163, 94.8124, and 96.0784, respectively. The precision of GWGHO-Deep LSTM model for the training percentage of 90%, with the epoch of 20, 40, 60, 80 and 100 are 83.5192, 85.4488, 88.1218, 95.5242, and 97.3996, respectively.

Figure 5 (c) shows the analysis in terms of recall. The recall of GWGHO-Deep LSTM model for the training percentage of 60%, with the epoch of 20, 40, 60, 80 and 100 are 89.4199, 90.7261, 91.1414, 91.8226, and 92.9161, respectively. The recall of GWGHO-Deep LSTM model for the training percentage of 70%, with the epoch of 20, 40, 60, 80 and 100 are 89.8527, 91.0371, 91.4575, 92.1913, and 93.0918, respectively. The recall of GWGHO-Deep LSTM model for the training percentage of 80%, with the epoch of 20, 40, 60, 80 and 100 are 89.9451, 91.2737, 91.4684, 92.3059, and 93.1468, respectively. The recall of GWGHO-Deep LSTM model for the training percentage of 90%, with the epoch of 20, 40, 60, 80 and 100 are 90.1042, 91.4099, 91.471, 92.4614, and 93.9053, respectively.

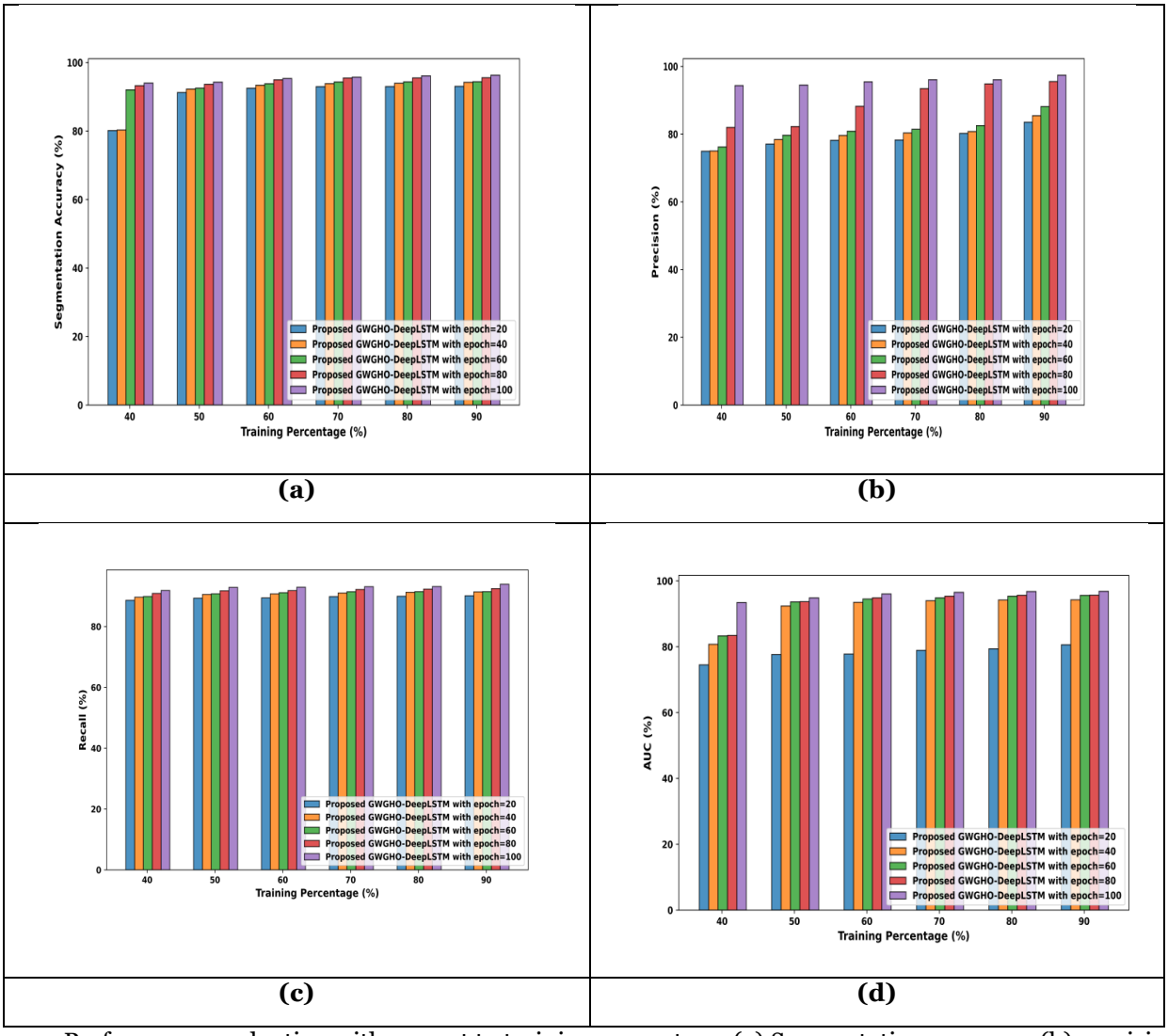

Figure 5. Performance evaluation with respect to training percentage, (a) Segmentation accuracy, (b) precision, (c) recall, and (d) AUC

The analysis is presented in terms of AUC in Figure 5(d). The AUC of GWGHO-Deep LSTM model for the training percentage of 60%, with the epoch of 20, 40, 60, 80 and 100 are 77.7603, 93.4846, 94.5069, 94.8407, and 96.0253, respectively. The AUC of GWGHO-Deep LSTM model for the training percentage of 70%, with the epoch of 20, 40, 60, 80 and 100 are 78.8936, 93.9705, 94.8388, 95.3465, and 96.5385, respectively. The AUC of GWGHO-Deep LSTM model for the training percentage of 80%, with the epoch of 20, 40, 60, 80 and 100 are 79.3559, 94.1923, 95.3356, 95.6336, and 96.7733, respectively. The AUC of GWGHO-Deep LSTM model for the training percentage of 90%, with the epoch of 20, 40, 60, 80 and 100 are 80.6016, 94.2471, 95.5834, 95.6507, and 96.8331, correspondingly.

4.5.3 Evaluation in terms of k-fold value

The evaluation of GWGHO-Deep LSTM in terms of precision, accuracy, recall, and AUC with respect to k-fold is portrayed in figure 6. Figure 6 (a) portrays the evaluation in terms of accuracy. The accuracy of GWGHO-Deep LSTM model for the k-fold of 2, with the epoch of 20, 40, 60, 80 and 100 are 74.3573, 83.2743, 90.6283, 92.0182, and 93.3708, respectively. The accuracy of GWGHO-Deep LSTM model for the k-fold of 3, with the epoch of 20, 40, 60, 80 and 100 are 78.3059, 89.6237, 90.768, 92.0552, and 93.9872, respectively. The accuracy of GWGHO-Deep LSTM model for the k-fold of 4%, with the epoch of 20, 40, 60, 80 and 100 are 83.1692, 90.4024, 91.1893, 92.5107, and 94.3901, respectively. The accuracy of GWGHO-Deep LSTM model for the k-fold of 5%, with the epoch of 20, 40, 60, 80 and 100 are 89.5057, 90.7577, 92.5415, 92.8933, and 94.8641, correspondingly.

Figure 6(b) shows the assessment in terms of accuracy. The precision of GWGHO-Deep LSTM model for the k-fold of 2, with the epoch of 20, 40, 60, 80 and 100 are 82.949, 83.4156, 91.4418, 92.1616, and 93.6991, respectively.

The precision of GWGHO-Deep LSTM model for the k-fold of 3, with the epoch of 20, 40, 60, 80 and 100 are 89.578, 90.0297, 92.6127, 92.6357, and 95.0188, respectively. The precision of GWGHO-Deep LSTM model for the k-fold of 4, with the epoch of 20, 40, 60, 80 and 100 are 90.0577, 91.363, 93.5271, 95.1149, and 95.5425, respectively. The precision of GWGHO-Deep LSTM model for the k-fold of 5, with the epoch of 20, 40, 60, 80 and 100 are 91.2823, 91.367, 93.7886, 95.633, and 96.1133, correspondingly.

The recall evaluation is demonstrated in Figure 6(c). The recall of GWGHO-Deep LSTM model for the k-fold of 2, with the epoch of 20, 40, 60, 80 and 100 are 76.326, 83.1626, 89.6532, 91.3217, and 92.5609, respectively. The recall of GWGHO-Deep LSTM model for the k-fold of 3, with the epoch of 20, 40, 60, 80 and 100 are 76.7059, 88.0829, 89.6579, 91.7201, and 93.6907, respectively. The recall of GWGHO-Deep LSTM model for the k-fold of 4, with the epoch of 20, 40, 60, 80 and 100 are 77.6232, 89.5232, 90.2956, 92.4278, and 93.9495, respectively. The recall of GWGHO-Deep LSTM model for the k-fold of 5, with the epoch of 20, 40, 60, 80 and 100 are 77.7681, 90.0852, 90.6856, 92.6451, and 94.655, correspondingly.

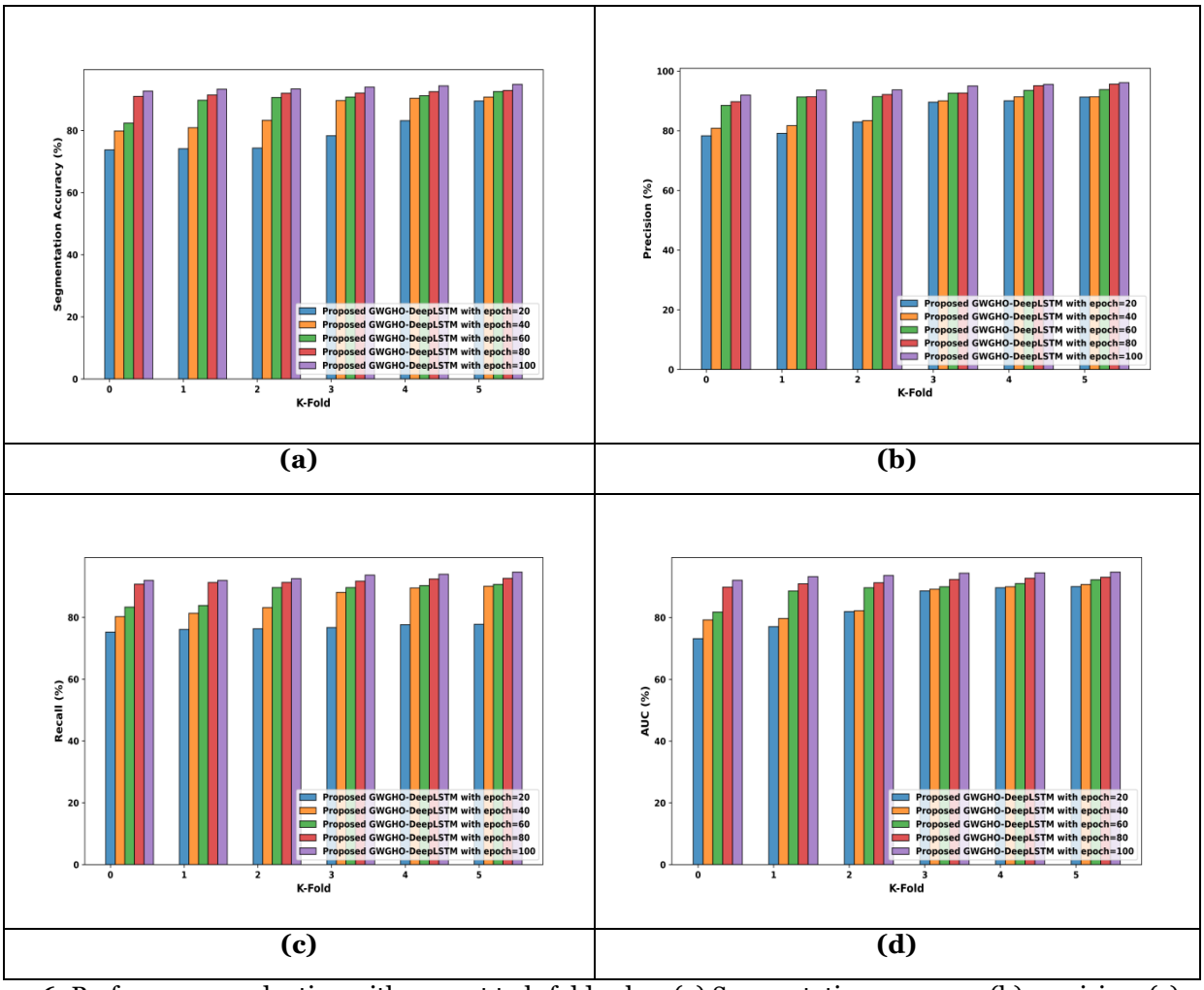

Figure 6. Performance evaluation with respect to k-fold value, (a) Segmentation accuracy, (b) precision, (c) recall, and (d) AUC

Figure 6 (d) depicts the evaluation in terms of ROC. The ROC of GWGHO-Deep LSTM model for the k-fold of 2, with the epoch of 20, 40, 60, 80 and 100 are 81.9448, 82.2067, 89.6686, 91.301, and 93.6293, respectively. The ROC of GWGHO-Deep LSTM model for the k-fold of 3, with the epoch of 20, 40, 60, 80 and 100 are 88.6562, 89.196, 90.0082, 92.3425, and 94.3961, respectively. The ROC of GWGHO-Deep LSTM model for the k-fold of 4, with the epoch of 20, 40, 60, 80 and 100 are 89.6612, 89.9905, 91.0069, 92.7314, and 94.4908, respectively. The ROC of GWGHO-Deep LSTM model for the k-fold of 5, with the epoch of 20, 40, 60, 80 and 100 are 90.0571, 90.7362, 92.2659, 93.0632, and 94.7329, respectively.

4.6 Comparative assessment

The comparative analysis of techniques used to segment chest CT images is covered in this section. Decision tree (DT) [33], support vector machine (SVM) [32], Adaboost classifier [34], CNN [35], and Deep convolutional neural network (DCNN) [36] are the approaches currently in use that are compared to the suggested GWGHO-Deep LSTM.

4.6.1 Comparative evaluation of training rates

Figure 7 shows a comparison of technique evaluations based on training %. Figure 7(a) shows the comparative evaluation in terms of accuracy. For a training percentage of 50%, the accuracy of techniques like SVM, DT, Adaboost, CNN, DCNN, and the proposed GWGHO-Deep LSTM model is 70.8253, 85.5212, 81.4921, 86.5176, 90.0129, and 91.2974, respectively. The accuracy of the methods, such as SVM, DT, Adaboost, CNN, DCNN, and the proposed GWGHO-Deep LSTM model for the training percentage of 60% is 72.8698, 86.8184, 82.994, 87.741, 91.3355, and 92.658, respectively. The accuracy of the methods, such as SVM, DT, Adaboost, CNN, DCNN, and the proposed GWGHO-Deep LSTM model for the training percentage of 70% is 74.1795, 87.341, 83.7449, 87.8148, 91.96, and 93.3073, respectively. For a training percentage of 80%, the accuracy of several approaches, including SVM, DT, Adaboost, CNN, DCNN, and the proposed GWGHO-Deep LSTM model, is, respectively, 83.3828, 88.4398, 87.0002, 89.0315, 91.9895, and 93.3511.

Figure 7(b) shows the comparative evaluation in terms of accuracy. For a training percentage of 50%, the precision of several approaches, including SVM, DT, Adaboost, CNN, DCNN, and the proposed GWGHO-Deep LSTM model, is as follows: 72.2953, 75.6541, 73.7805, 84.0008, 86.0411, and 87.8148. For a training percentage of 60%, the accuracy of the SVM, DT, Adaboost, CNN, DCNN, and suggested GWGHO-Deep LSTM model is 73.2392, 76.4041, 74.0766, 84.5892, 86.0703, and 89.112 correspondingly. The precision of the methods, such as SVM, DT, Adaboost, CNN, DCNN, and the proposed GWGHO-Deep LSTM model for the training percentage of 70% is 73.6322, 76.5848, 74.5772, 84.8269, 86.6094, and 90.4092, respectively. For an 80% training rate, the accuracy of several approaches, including SVM, DT, Adaboost, CNN, DCNN, and the proposed GWGHO-Deep LSTM model, is calculated as follows: 74.4726, 79.2706, 76.9296, 85.5487, 86.8184, and 90.5825.

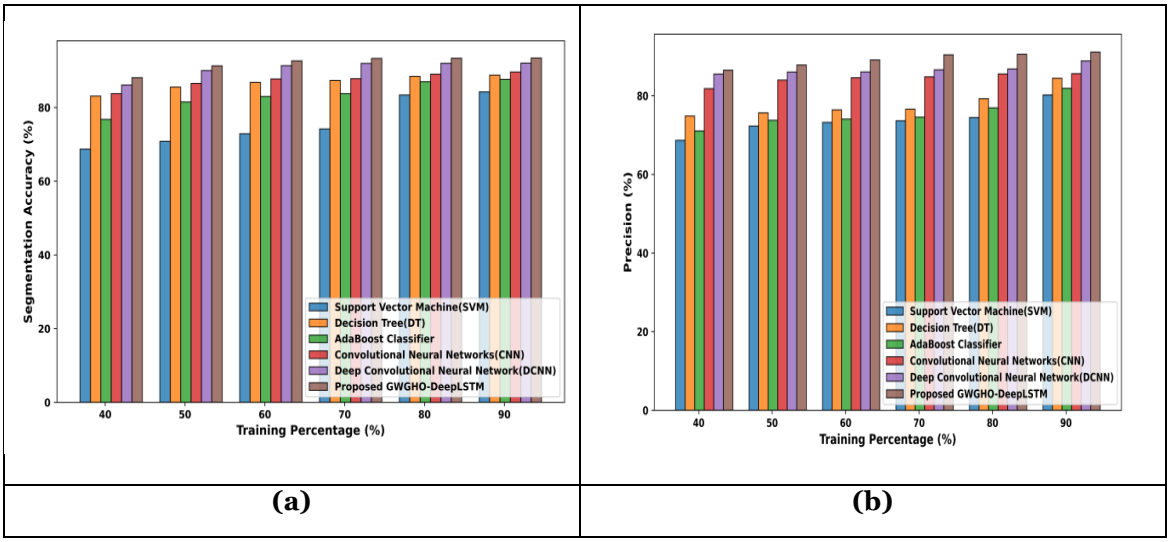

(a) **(b)**

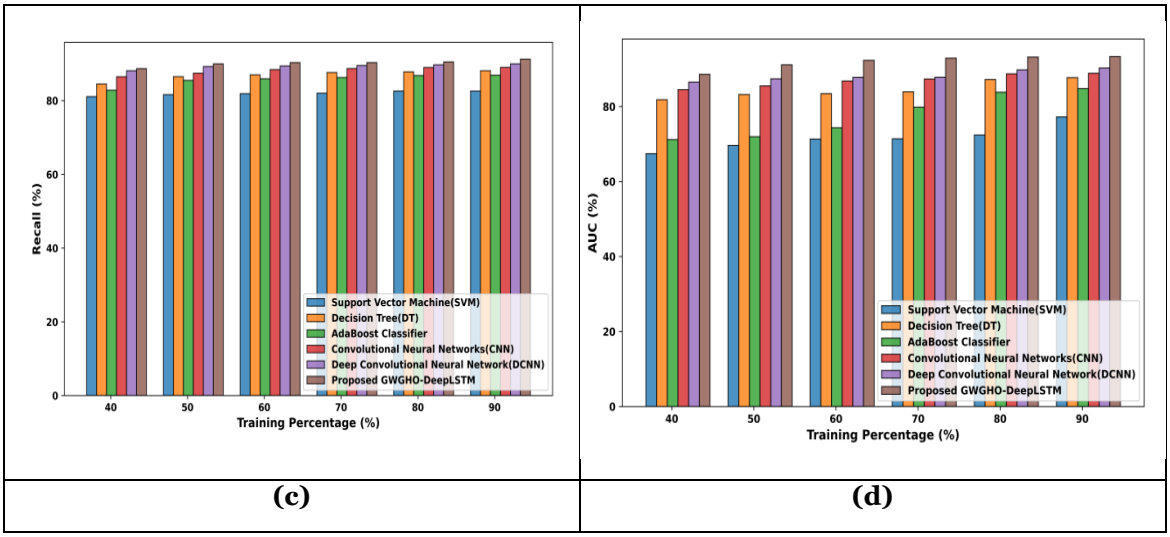

Figure 7. Comparative study of training %, (a) Segmentation accuracy, (b) precision, (c) recall, (d) AUC

Figure 7(c) shows the comparative assessment with regard to of recall. For a training percentage of 50%, the recall for the SVM, DT, Adaboost, CNN, DCNN, and suggested GWGHO-Deep LSTM model is 81.6355, 86.5176, 85.5212, 87.4509, 89.2607, and 90.0011, respectively. For a training percentage of 60%, the recall for the techniques SVM, DT, Adaboost, CNN, DCNN, and the proposed GWGHO-Deep LSTM model is 81.8969, 87.0149, 85.942, 88.4286, 89.4128, and 90.3414, respectively. For a training percentage of 70%, the recall for the techniques SVM, DT, Adaboost, CNN, DCNN, and the proposed GWGHO-Deep LSTM model is 82.0241, 87.6452, 86.2894, 88.7263, 89.565, and 90.3433, respectively. For an 80% training rate, the recall of several approaches, including SVM, DT, Adaboost, CNN, DCNN, and the proposed GWGHO-Deep LSTM model, is, respectively, 82.5993, 87.8148, 86.8184, 89.018, 89.7282, and 90.5175.

Figure 7(c) shows the comparative assessment in terms of AUC. For a 50% training rate, the AUC of several approaches, including SVM, DT, Adaboost, CNN, DCNN, and the proposed GWGHO-Deep LSTM model, is 69.6369, 83.2108, 71.9587, 85.5212, 87.4079, and 91.1392, respectively. The AUC of the methods, such as SVM, DT, Adaboost, CNN, DCNN, and the proposed GWGHO-Deep LSTM model for the training percentage of 60% is 71.3303, 83.4484, 74.3459, 86.8184, 87.7988, and 92.3333, respectively. For a 70% training rate, the AUC for several approaches, including SVM, DT, Adaboost, CNN, DCNN, and the proposed GWGHO-Deep LSTM model, is 71.4116, 83.9302, 79.839, 87.356, 87.8148, and 92.9004, respectively. For an 80% training rate, the AUC of several approaches, including SVM, DT, Adaboost, CNN, DCNN, and the proposed GWGHO-Deep LSTM model, is, respectively, 72.4073, 87.2168, 83.8059, 88.7339, 89.7873, and 93.2032.

4.6.2 Comparative evaluation using the k-fold value

Figure 8 illustrates the comparison of approaches' k-fold evaluations. Figure 8(a) displays the comparison analysis based on accuracy. For the k-fold value of 4, the accuracy of several techniques including SVM, DT, Adaboost, CNN, DCNN, and the proposed GWGHO-Deep LSTM model is 75.4214, 84.372, 80.6495, 86.1295, 90.5703, and 93.0215, respectively. For the k-fold value of 5, the accuracy of the various approaches, including SVM, DT, Adaboost, CNN, DCNN, and the proposed GWGHO-Deep LSTM model, is, respectively, 79.6121, 84.5462, 83.1588, 88.1002, 91.6764, and 93.807. For the k-fold number of 6, the accuracy of the various approaches, including SVM, DT, Adaboost, CNN, DCNN, and the proposed GWGHO-Deep LSTM model, is as follows: 81.6286, 86.4694, 84.8137, 89.1568, 92.4235, and 94.545. The accuracy of the methods, such as SVM, DT, Adaboost, CNN, DCNN, and the proposed GWGHO-Deep LSTM model for the k-fold value of 8 is 83.0558, 87.3913, 84.9838, 90.8941, 93.1221, and 96.1359, correspondingly.

Figure 8(b) shows the comparative assessment based on accuracy. For the k-fold number of 4, the accuracy of the various methods—including SVM, DT, Adaboost, CNN, DCNN, and the proposed GWGHO-Deep LSTM model—is, respectively, 74.8036, 84.5462, 80.5348, 86.1295, 90.5852, and 92.3831. The accuracy of the various approaches, including SVM, DT, Adaboost, CNN, DCNN, and the proposed GWGHO-Deep LSTM model, is 77.1579, 85.0953, 80.6859, 89.2465, 90.9011, and 93.744, respectively, for the k-fold value of 5. The accuracy of several techniques, including SVM, DT, Adaboost, CNN, DCNN, and the proposed GWGHO-Deep LSTM model, are,

respectively, 79.7304, 85.1522, 82.015, 90.4154, 91.0942, and 93.861 for the k-fold value of 6. The precision of the methods, such as SVM, DT, Adaboost, CNN, DCNN, and the proposed GWGHO-Deep LSTM model for the k-fold rate of 8 is 79.8443, 85.6304, 84.3933, 90.9737, 92.4031, and 96.4011, correspondingly.

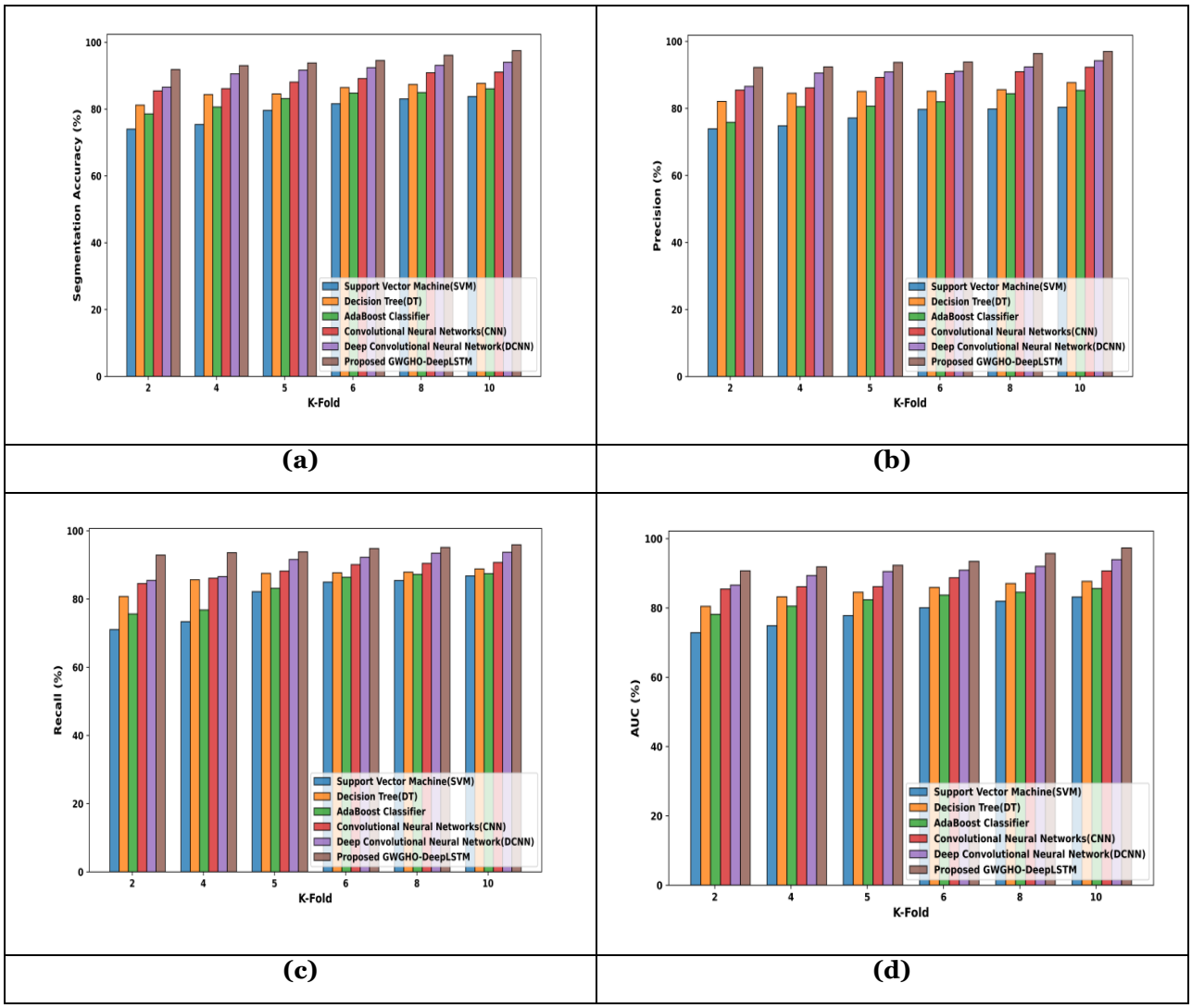

Figure 8. Comparative assessment using k-fold value, (a) Segmentation accuracy, (b) precision, (c) recall, (d) AUC

Figure 8(c) illustrates the comparative assessment based on recollection. For the k-fold value of 4, the recall for several techniques including SVM, DT, Adaboost, CNN, DCNN, and the proposed GWGHO-Deep LSTM model is 73.3835, 85.6667, 76.8228, 86.1295, 86.5922, and 93.5923, respectively. The recall for several algorithms, including SVM, DT, Adaboost, CNN, DCNN, and the proposed GWGHO-Deep LSTM model, is 82.1827, 87.5445, 83.1607, 88.2128, 91.6171, and 93.8454, respectively, for the k-fold rate of 5. For the k-fold rate of 6, the recall for several approaches including SVM, DT, Adaboost, CNN, DCNN, and the proposed GWGHO-Deep LSTM model is as follows: 84.9817, 87.7128, 86.3958, 90.109, 92.2579, and 94.8331. The recall of the methods, such as SVM, DT, Adaboost, CNN, DCNN, and the proposed GWGHO-Deep LSTM model for the k-fold value of 8 is 85.4523, 87.9095, 87.25, 90.4761, 93.4684, and 95.1565, correspondingly.

Table 2. Comparative discussion

S.No	Evaluation means	Metrics	Methods					
			SVM	DT	Adaboost	DCNN	DCNN	Proposed GWGHO-Deep LSTM
	Training percentage	**Accuracy (%)**	84.2292	88.7681	87.6422	89.6088	92.0396	93.4164

1		**Precision (%)**	80.2258	84.4593	81.8961	85.6195	88.8598	91.1133
		Recall (%)	82.6086	88.1156	86.9197	89.0460	89.9907	91.2644
		AUC (%)	77.2505	87.7097	84.7882	88.8862	90.2984	93.3369
2	**K-fold value**	**Accuracy (%)**	83.7817	87.7128	86.0753	91.1021	94.0383	97.5226
		Precision (%)	80.3598	87.7128	85.3902	92.3068	94.2413	96.9988
		Recall (%))	86.7873	88.8334	87.4573	90.7499	93.7446	95.9149
		AUC (%)	83.1711	87.7128	85.6304	90.6890	93.9609	97.3236

Figure 8(c) shows the comparative assessment based on AUC. For the k-fold value of 4, the AUCs of several approaches, including SVM, DT, Adaboost, CNN, DCNN, and the proposed GWGHO-Deep LSTM model, are, respectively, 74.8609, 83.2153, 80.5348, 86.1295, 89.3694, and 91.8883. For the k-fold value of 5, the AUC of the various methods—including SVM, DT, Adaboost, CNN, DCNN, and the proposed GWGHO-Deep LSTM model—is, respectively, 77.7935, 84.5462, 82.3743, 86.1549, 90.5219, and 92.3137. For the k-fold number of 6, the AUCs of several approaches, including SVM, DT, Adaboost, CNN, DCNN, and the proposed GWGHO-Deep LSTM model, are, respectively, 80.0696, 85.9334, 83.7307, 88.7114, 90.9029, and 93.4585. The AUC of the methods, such as SVM, DT, Adaboost, CNN, DCNN, and the proposed GWGHO-Deep LSTM model for the k-fold value of 8 is 81.9539, 87.0778, 84.5516, 90.0169, 92.0162, and 95.7412, respectively.

Table 2 contains the comparative analysis of the techniques used to segment chest CT images. From the evaluation, it is identified that the GWGHO-Deep LSTM model assist in the segmentation process with enhanced accuracy, precision, recall, and AUC as compared to the existing methods.

4.6.3 Comparison with state-of-art techniques

In this module, the performances achieved by the developed model are compared with the state-of-approaches like DNN, DTL, ResNet-50, XCOVNet, DiCNN, CSVM, MCNN, IDCNN, and 3D U-Net. Here, the performances including accuracy, recall, precision, and specificity are compared and validated with these techniques. Figure 9 portrays the comparison of proposed model performance with the state-of-art techniques. Fig 9 (a) illustrate the accuracy comparison. The state-of-art techniques including DNN, DTL, ResNet-50, XCOVNet, DiCNN, CSVM, MCNN, IDCNN, and 3D U-Net attained accuracy 87.5%, 90.2%, 90.8%, 86.3%, 89.7%, 84.6%, 88.9%, and 84.6%, respectively. The presented approach achieved an approximate accuracy of 95.46%.

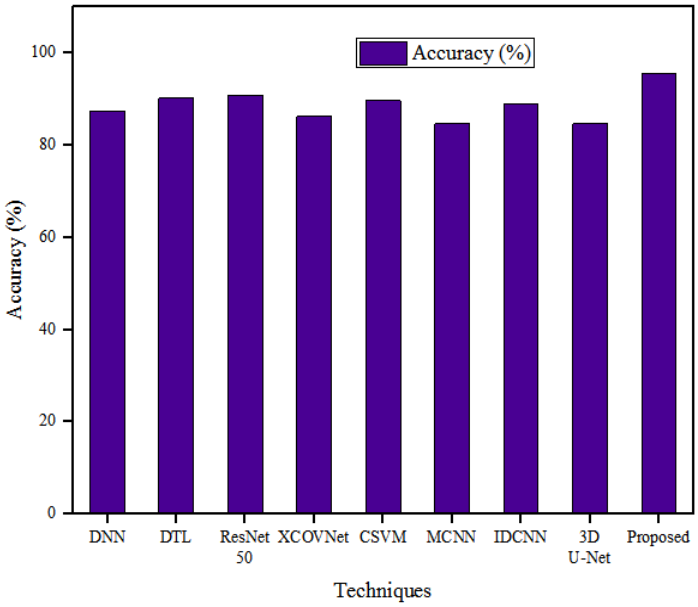

(a)

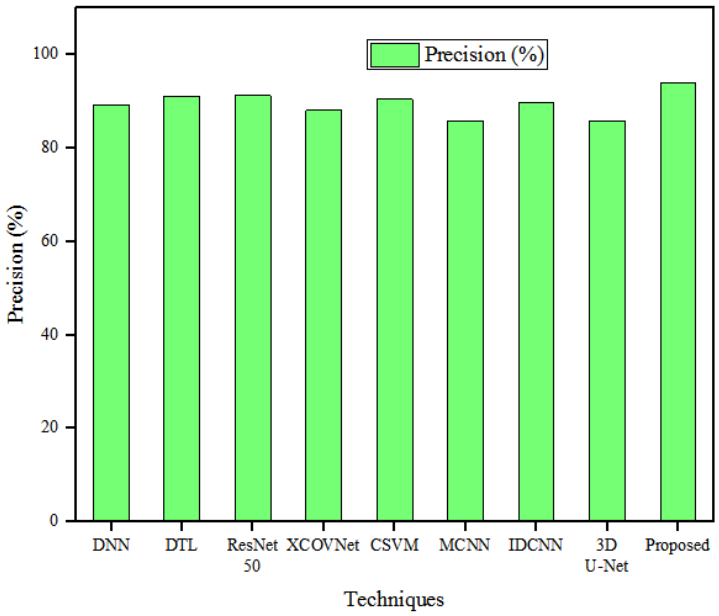

(b)

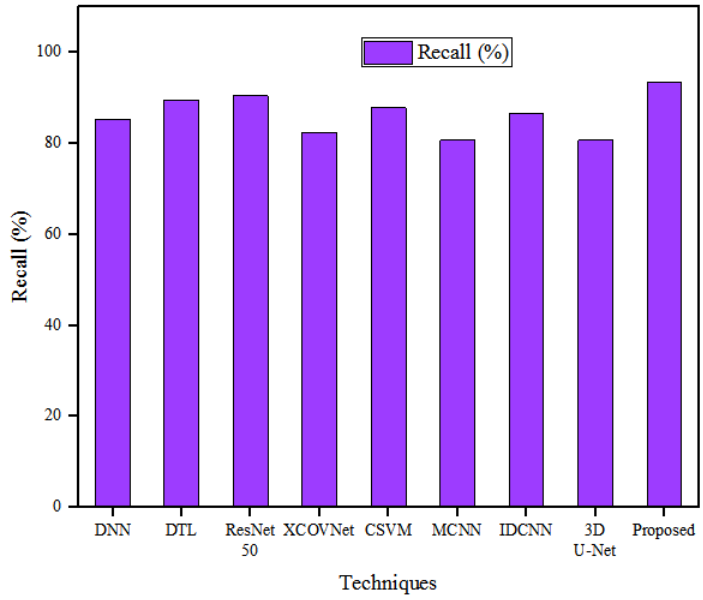

(c)

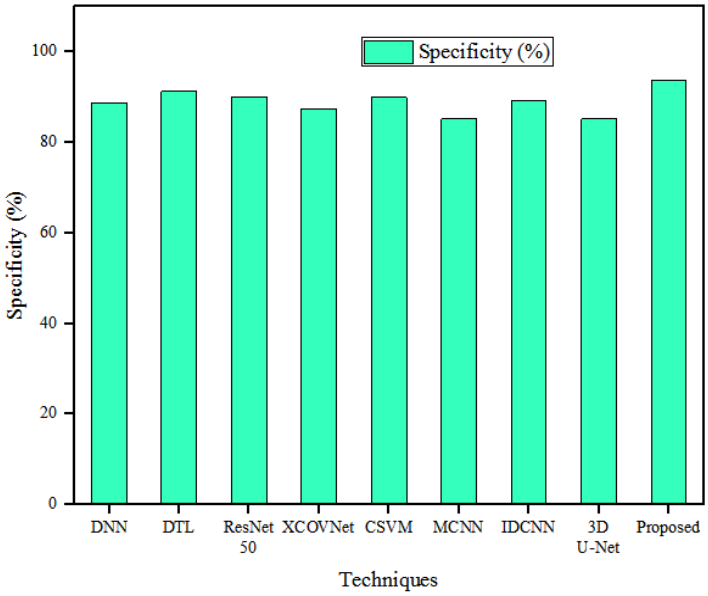

(d)

Figure.9 Comparison with state-of-art approaches: (a) accuracy, (b) precision, (c) recall, and (d) specificity

The comparison of precision with state-of-art models is displayed in figure 9 (b). The approaches like DNN, DTL, ResNet-50, XCOVNet, DiCNN, CSVM, MCNN, IDCNN, and 3D U-Net obtained precision rate of 89.3%, 89.6%, 90.5%, 82.4%, 87.9%, 80.7%, 86.5%, and 83.8%, respectively. But the presented technique attained precision of 93.58%, which is greater compared to the state-of-art models. Figure 9 (c) displays the recall comparison. The methods including DNN, DTL, ResNet-50, XCOVNet, DiCNN, CSVM, MCNN, IDCNN, and 3D U-Net earned 85.2%, 89.6%, 90.5%, 82.4%, 87.9%, 80.7%, 86.5%, and 83.8%, respectively. The proposed model attained an average recall rate of 93.58%. Figure 9 (d) displays the specificity comparison. The state-of-art models like DNN, DTL, ResNet-50, XCOVNet, DiCNN, CSVM, MCNN, IDCNN, and 3D U-Net obtained specificity percentage of 88.7%, 91.3%, 90.1%, 87.5%, 90%, 85.2%, 89.2%, and 83.2%, respectively. The developed technique earned 93.85%; this illustrates that the designed model obtained greater performance compared to the above-mentioned state-of-art techniques.

Table 3 Comparison with state-of-art techniques

Techniques	Accuracy (%)	Recall (%)	Precision (%)	Specificity (%)
DNN	87.5	85.2	89.3	88.7
DTL	90.2	89.6	91.1	91.3
ResNet 50	90.8	90.5	91.3	90.1
XCOVNet	86.3	82.4	88.1	87.5
CSVM	89.7	87.9	90.5	90
MCNN	84.6	80.7	85.8	85.2
IDCNN	88.9	86.5	89.7	89.2
3D U-Net	84.6	83.8	84.8	83.2
Proposed	95.46	93.58	94.05	93.85

The comparative study illustrates that the designed technique exhibited superior performance compared to the conventional state-of-art approaches for the task of COVID-19 CT chest image classification. The greater accuracy, recall, specificity, and precision obtained by the designed technique signify its efficiency in correctly classifying COVID-19 cases from CT images. Table 3 lists the overall comparative analysis with the state-of-art methods. These findings verify that the designed model has greater potential in clinical practice and patient management.

4.7 Discussion

This study presented hybrid optimization tuned deep LSTM algorithm for the timely detection of COVID-10 lesions in chest CT images. The framework was developed to address the need for quick and accuracy diagnosis of COVID-19 cases from the chest images. The diagnosis process begins with the collection of CT images containing both normal and COVID-19 infected chest images. The acquired image database undergoes pre-processing mechanism, which includes image resizing, contrast enhancement, normalization, and standardization. This process confirms that all images available in the collected database have same dimensions and intensity range. The pre-processed CT images are then segmented using the hybrid optimization tuned deep LSTM model. This proposed framework integrates the benefits of deep LSTM and GWGHO algorithms for effective lesion segmentation. The deep LSTM architecture enables the system to capture spatial dependencies and temporal data within the images effectively and provides accurate lesion segmentation. In addition, the integrated hybrid optimization GWGHO iteratively fine-tunes and optimizes the hyperparameters of deep LSTM including weights, network depth, number of layers, learning rate, batch size, etc., to enhance the segmentation precision. This hybrid optimization –based tuning process provides combined benefits of grey wolves exploration and grasshopper exploitation capacities. This algorithm searches for the optimal sequence of hyperparameters for the deep LSTM model to improve the segmentation efficiency. This improved segmentation efficiency of the system demonstrates that the developed model can potentially distinguish the COVID-19 lesions from the surrounding healthy tissues, leading to more reliable and accurate results. In addition, the developed model can classify the different types of COVID-19 lesions by utilizing the diverse and high quality dataset for training purpose. The training of developed model using the diverse dataset containing CT images of different types of lesions enables us to categorize the different lesion types accurately. This training process requires a training database, which covers wide range of lesion types and includes ground-truth annotations indicating the presence and location of different lesion types. The intensive training, the developed model can detect the types of COVID-19 lesion accurately. Thus, the developed model can be applied to real-world scenarios for COVID-19 lesion prediction.

Therefore, the proposed model can be seamlessly integrated into the existing medical imaging system to support the radiologists in COVID-19 lesion segmentation and helps to provide effective measures for disease monitoring and treat evaluation. Using the proposed framework, the radiologist can simply upload the chest CT images into the software and the integrated module performs lesion segmentation using the optimized deep LSTM algorithm. Finally, the module produces the segmented images enabling the radiologist to assess disease progression and treatment. This seamless integration of proposed work in the clinical practices has potential implications including early detection and diagnosis, enables faster and reliable assessment, support decision-making, effective treat planning and monitoring, reduces workload, and provides personalized treatment process. By aiding radiologists in lesion

segmentation, the model contributes to effective disease monitoring and treatment evaluation, leading to better management of COVID-19 patients. Thus, the presented framework acts a powerful mechanism for early identification of COVID-19. At last, the efficiency and performances of the proposed model were analyzed in terms of different training percentage and k-fold value. The high accuracy and minimum loss in the training and validation process manifest the convergence speed and robustness of the proposed model. Furthermore, the models effectiveness was evaluated by segmenting the CT images with different severity range and the segmented images are compared within actual label images to assess the models precision and reliability.

However, the proposed model lacks interoperability and explainability and these issues can be resolved by utilizing the attention mechanisms. This utilization mechanism makes the system's decision-making process transparent and provides visualization regarding the important attributes employed for lesion segmentation. In addition, comparing the segmented outcomes with the clinical results improves transparency. The utilization of these mechanisms' enables the radiologists and clinicians to understand and trust the segmentation outputs, aiding diagnostic interpretation for COVID-19 patients. In addition to this, the real-time implementation of the proposed work in clinical practice poses certain limitations including need for interpretability, low generalizability across diverse patient populations and imaging protocols. In addition, the developed model ace challenges imaging variability, patient population, lesion variability, labeling variability, etc. To overcome these limitations, a robust training on diverse databases should be given to the proposed work; this makes the system efficient for real-time COVID-19 lesion segmentation with increased cross dataset performance.

5. Conclusion

For the purpose of to segment Chest CT images and identify COVID-19 patients, this research suggests a unique Grey wolf-Grasshopper optimisation (GWGHO) optimised Deep Long short term memory (Deep-LSTM) model. By optimising the weights of the Deep-LSTM, the GWGHO, an integration of the characteristics of grey wolves and grasshoppers, plays a significant part in improving the effectiveness of the suggested segmentation model. Segmentation accuracy, recall, precision, and AUC are the evaluation indices used to evaluate the effectiveness of the GWGHO-Deep LSTM approach. When compared to the current approaches, the segmentation accuracy of the proposed GWGHO-Deep LSTM is high at 97.5226%. To further improve the segmentation accuracy of the suggested model, the segmentation procedure will be carried out in the future employing ensemble classifiers.

Compliance with Ethical Standards

Conflict of interest

The authors declare that they have no conflict of interest.

Human and Animal Rights

This article does not contain any studies with human or animal subjects performed by any of the authors.

Informed Consent

Informed consent does not apply as this was a retrospective review with no identifying patient information.

Funding: Not applicable

Conflicts of interest Statement: Not applicable

Consent to participate: Not applicable

Consent for publication: Not applicable

Availability of data and material:

Data sharing is not applicable to this article as no new data were created or analyzed in this study.

Code availability: Not applicable

References

[1] Selvaraj, Deepika, Arunachalam Venkatesan, Vijayalakshmi GV Mahesh, and Alex Noel Joseph Raj. "An integrated feature frame work for automated segmentation of COVID-19 infection from lung CT images." International Journal of Imaging Systems and Technology 31, no. 1 (2021): 28-46.

[2] Suri, Jasjit S., Sushant Agarwal, Pranav Elavarthi, Rajesh Pathak, Vedmanvitha Ketireddy, Marta Columbu, Luca Saba et al. "Inter-Variability Study of COVLIAS 1.0: Hybrid Deep Learning Models for COVID-19 Lung Segmentation in Computed Tomography." Diagnostics 11, no. 11 (2021): 2025.

[3] Minaee, Shervin, Rahele Kafieh, Milan Sonka, Shakib Yazdani, and Ghazaleh Jamalipour Soufi. "Deep-covid: Predicting covid-19 from chest x-ray images using deep transfer learning." Medical image analysis 65 (2020): 101794.

[4] Goldstein, Elisha, Daphna Keidar, Daniel Yaron, Yair Shachar, Ayelet Blass, Leonid Charbinsky, Israel Aharony et al. "Covid-19 classification of x-ray images using deep neural networks." arXiv preprint arXiv:2010.01362 (2020).

[5] Madaan, Vishu, Aditya Roy, Charu Gupta, Prateek Agrawal, Anand Sharma, Cristian Bologa, and Radu Prodan. "XCOVNet: Chest X-ray Image Classification for COVID-19 Early Detection Using Convolutional Neural Networks." New Generation Computing (2021): 1-15.

[6] Kumar, Shailender, Kumar Abhishek, and Kashish Singh. "COVID-19 Detection from Chest X-Rays and CT Scans using Dilated Convolutional Neural Networks." In 2021 10th IEEE International Conference on Communication Systems and Network Technologies (CSNT), pp. 369-374. IEEE, 2021.

[7] Özkaya, Umut, Şaban Öztürk, Serkan Budak, Farid Melgani, and Kemal Polat. "Classification of COVID-19 in Chest CT Images using Convolutional Support Vector Machines." arXiv preprint arXiv:2011.05746 (2020).

[8] Hussain, Md Gulzar, and Ye Shiren. "Recognition of COVID-19 Disease Utilizing X-Ray Imaging of the Chest Using CNN." In 2021 International Conference on Computing, Electronics & Communications Engineering (iCCECE), pp. 71-76. IEEE, 2021.

[9] Kwee, Thomas C., and Robert M. Kwee. "Chest CT in COVID-19: what the radiologist needs to know." RadioGraphics 40, no. 7 (2020): 1848-1865.

[10] Awal, Md Abdul, Mehedi Masud, Md Shahadat Hossain, Abdullah Al-Mamun Bulbul, SM Hasan Mahmud, and Anupam Kumar Bairagi, "A novel bayesian optimization-based machine learning framework for COVID-19 detection from inpatient facility data", IEEE Access, vol. 9, pp.10263-10281, 2021.

[11] Abbas, Asmaa, Mohammed M. Abdelsamea, and Mohamed Medhat Gaber, "Classification of COVID-19 in chest X-ray images using DeTraC deep convolutional neural network", Applied Intelligence 51, no. 2, pp. 854-864, 2021.

[12] Syrjala, Hannu, Markku Broas, Pasi Ohtonen, Airi Jartti, and Eija Pääkkö. "Chest magnetic resonance imaging for pneumonia diagnosis in outpatients with lower respiratory tract infection." European Respiratory Journal 49, no. 1 (2017).

[13] Gupta, Shubham, Vishal Bharti, and Anil Kumar. "A survey on various machine learning algorithms for disease prediction." Int. J. Recent Technol. Eng 7, no. 6c (2019): 84-87.

[14] Aguiar, Diego, Johannes Alexander Lobrinus, Manuel Schibler, Tony Fracasso, and Christelle Lardi. "Inside the lungs of COVID-19 disease." International Journal of Legal Medicine 134 (2020): 1271-1274.

[15] Tahamtan, Alireza, and Abdollah Ardebili. "Real-time RT-PCR in COVID-19 detection: issues affecting the results." Expert review of molecular diagnostics 20, no. 5 (2020): 453-454.

[16] Maguolo, Gianluca, and Loris Nanni. "A critic evaluation of methods for covid-19 automatic detection from x-ray images." Information Fusion 76 (2021): 1-7.

[17] Tenda, Eric D., Mira Yulianti, M. Asaf, R. Yunus, Wita Septiyanti, Vally Wulani, Ceva W. Pitoyo, Cleopas M. Rumende, and Siti Setiati. "The importance of chest CT scan in COVID-19: A case series." Acta med indones 52, no. 1 (2020): 68-73.

[18] Peeling, Rosanna W., Piero L. Olliaro, Debrah I. Boeras, and Noah Fongwen. "Scaling up COVID-19 rapid antigen tests: promises and challenges." The Lancet infectious diseases (2021).

[19] Ghaffari, Abdi, Robyn Meurant, and Ali Ardakani. "COVID-19 serological tests: how well do they actually perform?." Diagnostics 10, no. 7 (2020): 453.

[20] Xiao, Ai Tang, Yi Xin Tong, and Sheng Zhang. "False-negative of RT-PCR and prolonged nucleic acid conversion in COVID-19: rather than recurrence." Journal of medical virology (2020).

[21] Feng, Hao, Yujian Liu, Minli Lv, and Jianquan Zhong. "A case report of COVID-19 with false negative RT-PCR test: necessity of chest CT." Japanese journal of radiology 38, no. 5 (2020): 409-410.
[22] Khosravi, Bardia, Leila Aghaghazvini, Majid Sorouri, Sara Naybandi Atashi, Mohammad Abdollahi, Helia Mojtabavi, Marjan Khodabakhshi et al. "Predictive value of initial CT scan for various adverse outcomes in patients with COVID-19 pneumonia." Heart & Lung 50, no. 1 (2021): 13-20.
[23] Tabik, Siham, Anabel Gómez-Ríos, José Luis Martín-Rodríguez, Iván Sevillano-García, Manuel Rey-Area, David Charte, Emilio Guirado et al. "COVIDGR dataset and COVID-SDNet methodology for predicting COVID-19 based on Chest X-Ray images." IEEE Journal of Biomedical and Health Informatics 24, no. 12 (2020): 3595-3605.
[24] Lei, Shaoqing, Fang Jiang, Wating Su, Chang Chen, Jingli Chen, Wei Mei, Li-Ying Zhan et al. "Clinical characteristics and outcomes of patients undergoing surgeries during the incubation period of COVID-19 infection." EClinicalMedicine 21 (2020): 100331.
[25] Polsinelli, Matteo, Luigi Cinque, and Giuseppe Placidi. "A light CNN for detecting COVID-19 from CT scans of the chest." Pattern recognition letters 140 (2020): 95-100.
[26] Khalifa, Nour Eldeen M., Gunasekaran Manogaran, Mohamed Hamed N. Taha, and Mohamed Loey. "A deep learning semantic segmentation architecture for COVID-19 lesions discovery in limited chest CT datasets." Expert Systems (2021): e12742.
[27] Demir, Fatih. "DeepCoroNet: A deep LSTM approach for automated detection of COVID-19 cases from chest X-ray images." Applied Soft Computing 103 (2021): 107160.
[28] Islam, Md Zabirul, Md Milon Islam, and Amanullah Asraf. "A combined deep CNN-LSTM network for the detection of novel coronavirus (COVID-19) using X-ray images." Informatics in medicine unlocked 20 (2020): 100412.
[29] Mirjalili, Seyedali, Shahrzad Saremi, Seyed Mohammad Mirjalili, and Leandro dos S. Coelho. "Multi-objective grey wolf optimizer: a novel algorithm for multi-criterion optimization." Expert Systems with Applications 47 (2016): 106-119.
[30] Mirjalili, Seyedeh Zahra, Seyedali Mirjalili, Shahrzad Saremi, Hossam Faris, and Ibrahim Aljarah. "Grasshopper optimization algorithm for multi-objective optimization problems." Applied Intelligence 48, no. 4 (2018): 805-820.
[31] Covid segmentation database, available on https://www.kaggle.com/c/covid-segmentation/data.
[32] Hu, Rongyao, Jiangzhang Gan, Xiaofeng Zhu, Tong Liu, and Xiaoshuang Shi. "Multi-task multi-modality SVM for early COVID-19 Diagnosis using chest CT data." Information Processing & Management 59, no. 1 (2022): 102782.
[33] Yoo, Seung Hoon, Hui Geng, Tin Lok Chiu, Siu Ki Yu, Dae Chul Cho, Jin Heo, Min Sung Choi et al. "Deep learning-based decision-tree classifier for COVID-19 diagnosis from chest X-ray imaging." Frontiers in medicine 7 (2020): 427.
[34] Sun, Liang, Zhanhao Mo, Fuhua Yan, Liming Xia, Fei Shan, Zhongxiang Ding, Bin Song et al. "Adaptive feature selection guided deep forest for covid-19 classification with chest ct." IEEE Journal of Biomedical and Health Informatics 24, no. 10 (2020): 2798-2805.
[35] Apostolopoulos, Ioannis D., and Tzani A. Mpesiana. "Covid-19: automatic detection from x-ray images utilizing transfer learning with convolutional neural networks." Physical and Engineering Sciences in Medicine 43, no. 2 (2020): 635-640.
[36] Narin, Ali, Ceren Kaya, and Ziynet Pamuk. "Automatic detection of coronavirus disease (covid-19) using x-ray images and deep convolutional neural networks." Pattern Analysis and Applications (2021): 1-14.
[37] Yan, Qingsen, Bo Wang, Dong Gong, Chuan Luo, Wei Zhao, Jianhu Shen, Qinfeng Shi, Shuo Jin, Liang Zhang, and Zheng You. "COVID-19 chest CT image segmentation--a deep convolutional neural network solution." arXiv preprint arXiv:2004.10987 (2020).
[38] Müller, Dominik, Iñaki Soto Rey, and Frank Kramer. "Automated chest ct image segmentation of covid-19 lung infection based on 3d u-net." arXiv preprint arXiv:2007.04774 (2020).